





# Experimental study of quasi-coherent mode using EAST tangential CO<sub>2</sub> laser collective scattering diagnostic in far-forward mode

Cite as: Phys. Plasmas **26**, 012304 (2019); <https://doi.org/10.1063/1.5049209>

Submitted: 20 July 2018 . Accepted: 12 November 2018 . Published Online: 10 January 2019

P. J. Sun , Y. D. Li, Y. Ren, X. D. Zhang, G. J. Wu, Y. M. Wang , T. H. Shi, B. Lyu , Y. M. Duan, J. Z. Zhang, F. D. Wang, H. Q. Liu , S. T. Mao, L. Q. Xu, Q. Li, P. Li, J. Bi, L. Q. Hu, and J. G. Li

## COLLECTIONS

 This paper was selected as an Editor's Pick



View Online



Export Citation



CrossMark

## ARTICLES YOU MAY BE INTERESTED IN

[Wavelet methods for studying the onset of strong plasma turbulence](#)

Phys. Plasmas **25**, 122310 (2018); <https://doi.org/10.1063/1.5062853>

[Nonlinear dynamics of shear Alfvén fluctuations in divertor tokamak test facility plasmas](#)

Phys. Plasmas **26**, 012504 (2019); <https://doi.org/10.1063/1.5064863>

[Hybrid simulations of fishbone instabilities and Alfvén eigenmodes in DIII-D tokamak](#)

Phys. Plasmas **25**, 122504 (2018); <https://doi.org/10.1063/1.5064647>



# Experimental study of quasi-coherent mode using EAST tangential CO<sub>2</sub> laser collective scattering diagnostic in far-forward mode

Cite as: Phys. Plasmas **26**, 012304 (2019); doi: 10.1063/1.5049209

Submitted: 20 July 2018 · Accepted: 12 November 2018 · Published Online: 10 January 2019



View Online



Export Citation



CrossMark

P. J. Sun,<sup>1,a)</sup>  Y. D. Li,<sup>1</sup> Y. Ren,<sup>2</sup> X. D. Zhang,<sup>1</sup> G. J. Wu,<sup>1</sup> Y. M. Wang,<sup>1</sup>  T. H. Shi,<sup>1</sup> B. Lyu,<sup>1</sup>  Y. M. Duan,<sup>1</sup> J. Z. Zhang,<sup>1</sup> F. D. Wang,<sup>1</sup> H. Q. Liu,<sup>1</sup>  S. T. Mao,<sup>1</sup> L. Q. Xu,<sup>1</sup> Q. Li,<sup>3</sup> P. Li,<sup>1</sup> J. Bi,<sup>1</sup> L. Q. Hu,<sup>1</sup> and J. G. Li<sup>1</sup>

## AFFILIATIONS

<sup>1</sup> Institute of Plasma Physics, Chinese Academy of Sciences, Hefei 230031, China

<sup>2</sup> Princeton Plasma Physics Laboratory, Princeton, New Jersey 08543, USA

<sup>3</sup> Guangdong University of Technology, Guangzhou 510006, China

a) sunpj@ipp.cas.cn

## ABSTRACT

A quasi-coherent mode (QCM) was measured by the tangential CO<sub>2</sub> laser collective scattering diagnostic at high plasma electron density during both enhanced D<sub>z</sub>/small edge-localized mode (ELM) and ELM-free H mode phases in Experimental Advanced Superconducting Tokamak (EAST). Experimental results from only local oscillator CO<sub>2</sub> laser scattering prove that the QCM is measured by the scattering diagnostic in the far-forward mode. The driven QCM density fluctuation ( $k_{\perp} < 3 \text{ cm}^{-1}$ ) and magnetic fluctuation suggest that the QCM is an electromagnetic mode. The typical frequency of the QCM is  $f \approx 26.5 \text{ kHz}$ . A combination analysis of scattering signals and Mirnov signals suggests that the QCM has toroidal mode number  $n \approx 17$  and rotates along with the electron diamagnetic drift velocity direction in the lab frame. The analysis of Mirnov and reflectometer signals supports that the QCM locates in the edge pedestal region. The QCM power has been found to be related to both the D<sub>z</sub> signal and the pedestal density gradient. A comparison of the EAST QCM and C-Mod quasi-coherent mode has been given in detail.

Published under license by AIP Publishing. <https://doi.org/10.1063/1.5049209>

## I. INTRODUCTION

Anomalous transport is a particularly important issue for magnetic confinement fusion devices, especially as predicted for ITER,<sup>1</sup> CFETR,<sup>2</sup> and future fusion reactors.<sup>3</sup> Microturbulence is generally considered to determine the consequent anomalous transport.<sup>4–9</sup> Multiple microinstabilities, with different drive force and time-spatial scales, can coexist and nonlinearly interplay with each other.<sup>10–13</sup> This can either lead to fully developed and nonlinearly saturated broadband turbulence or introduce new phenomena, e.g., a regular coherent mode<sup>14</sup> under specific circumstances in magnetized plasma. Such quasi-coherent modes, with well-defined frequency and poloidal/toroidal mode number  $m/n$ , have been observed in the high confinement edge/internal transport barrier (ETB/ITB) plasmas (being characterized by a steep density and/or temperature profile) for several magnetic fusion devices. In the poloidal divertor experiment (PDX) tokamak, a quasi-coherent mode (the frequency  $f$  is  $\sim 50$ – $180 \text{ kHz}$ , localized just inside the separatrix) was observed

by both the microwave collective scattering diagnostic and the CO<sub>2</sub> laser interferometer diagnostic in the H mode discharge.<sup>15</sup> In the TJ-II stellarator, the quasi-coherent mode in the plasma core has been investigated by HIBP during the formation of electron internal transport barriers.<sup>16</sup> In the C-mod tokamak, a steady quasi-coherent (QC) mode near the pedestal region with  $f \sim 100$ – $150 \text{ kHz}$  has been detected by Langmuir probe, phase contrast imaging, and edge reflectometer diagnostics during the enhanced D<sub>z</sub> (EDA) H mode phase, which has good core energy confinement and low edge particle confinement.<sup>17–22</sup> All these observations show that the quasi-coherent mode could be excited under specific circumstances (e.g., ITB/ETB) in magnetized plasma, and as a result, anomalous plasma transport can be affected. Detecting and further understanding these quasi-coherent modes are important for not only predicting and improving the confinement performance of future fusion devices but also their safe and steady state operations since predicting plasma transport with the existence of the unstable quasi-

coherent mode is very important. It is important to note that the C-Mod Quasi-coherent mode is not universally seen in every magnetic fusion device. This may be due to the lack of suitable diagnostics to detect it. In this paper, we present the study of the quasi-coherent mode (QCM) through using the Experimental Advanced Superconducting Tokamak (EAST) tangential CO<sub>2</sub> laser collective scattering diagnostic in the far-forward mode during EDA/small edge-localized mode (ELM) or ELM-free H mode phases for lower hybrid waves (LHW) alone or LHW coupled with ion cyclotron resonance frequency (ICRF) plasmas. It includes the identification of the QCM being measured by the local oscillator (LO) CO<sub>2</sub> laser far-forward scattering diagnostic, the observation of the quasi-coherent mode by the collective scattering system, and the comparison of the QCM in EAST with the QC mode in the C-Mod tokamak. These results can contribute to the development of the electromagnetic wave far-forward collective scattering diagnostic to measure the QCM and also can contribute to testing and improving theoretical models and simulations of turbulent transport in the presence of the QCM so that the physical mechanisms under plasma anomalous transport can be better understood.

This paper is organized as follows: Section II shows the EAST CO<sub>2</sub> laser collective scattering diagnostic in both forward and far-forward modes. Identification of the QCM being measured by LO CO<sub>2</sub> laser far-forward scattering is shown in Sec. III. In Sec. IV, we present experimental results and discussion, which includes an overview of EDA/small ELM H mode plasma discharge (see Sec. IVA), the observation of the QCM by the CO<sub>2</sub> laser collective scattering system (see Sec. IVB), and the comparison of the QCM in EAST with the QC mode in C-Mod tokamak (see Sec. IV C). Summary is given in Sec. V.

## II. EAST CO<sub>2</sub> LASER COLLECTIVE SCATTERING DIAGNOSTIC

Density fluctuations can be measured by the electromagnetic wave collective Thomson scattering diagnostic.<sup>23</sup> Scattered signals received from detector D, Fig. 1, are proportional to the spatial Fourier transform of density fluctuation at the wave vector  $\vec{k}$  with the scattering power  $P_s = \frac{1}{4} P_0 r_e^2 \tilde{n}_e^2 L_v^2$ , where  $P_0$ ,  $r_e$ ,  $\lambda_0$ ,  $\tilde{n}_e$ , and  $L_v$  are the incident power of the CO<sub>2</sub> laser (used to produce scattered signals), the classical electron radius, the wavelength of the incident laser, the electron density fluctuation, and the length of scattering volume, respectively. Both the frequency  $\omega$  and wave-vector  $\vec{k}$  of the measured density fluctuation must satisfy the energy and momentum conservation, e.g.,  $\omega = \omega_s - \omega_i$  and  $\vec{k} = \vec{k}_s - \vec{k}_i$ , where s and i refer to scattered and incident waves, respectively. The measurement of density fluctuation in this paper was carried out with the EAST tangential two-channel CO<sub>2</sub> laser (single mode TEM<sub>00</sub>) collective scattering diagnostic shown in Fig. 1. The CO<sub>2</sub> laser was divided into two local oscillator (LO1 and LO2) CO<sub>2</sub> lasers and a main beam (MB) CO<sub>2</sub> laser by using two beam splitters (BS1 and BS2). Both MB and LO CO<sub>2</sub> laser beams go through the plasmas. The MB CO<sub>2</sub> laser with power  $P_{MB} \approx 10$  W can produce forward scattering signals to measure the (intermediate and high)- $k$  ( $k_{\perp} = 10 - 30 \text{ cm}^{-1}$ ) density fluctuation with wavenumber

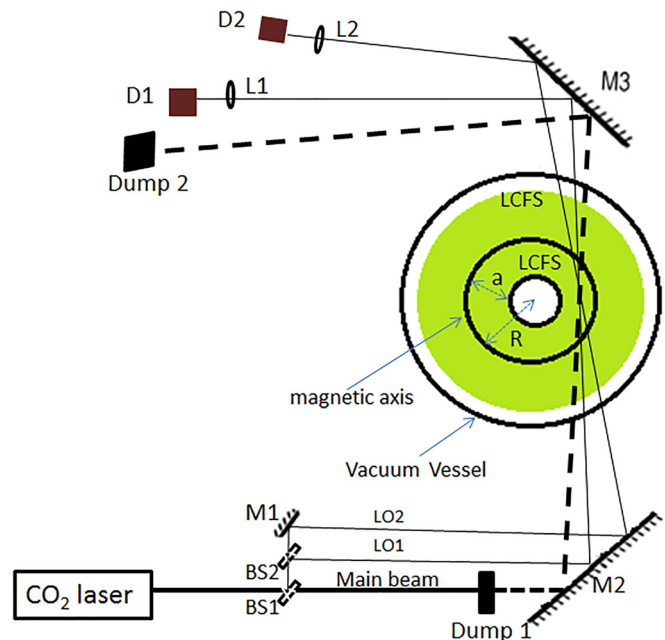


FIG. 1. A schematic of the tangential CO<sub>2</sub> laser collective scattering diagnostic on EAST, where “BS,” “M,” “LO,” “L,” and “D” represent the beam splitter, mirror, local oscillator, lens, and detector, respectively. Dump 1 and Dump 2 can be used to block the MB CO<sub>2</sub> laser before and after it goes through the plasmas, separately.

resolution  $\Delta k \approx 2 \text{ cm}^{-1}$  in the forward mode. Although the power,  $P_{LO} \leq 0.4 \text{ mW}$ , is extremely small, each LO CO<sub>2</sub> laser still can produce far-forward scattering signals to measure the low- $k$  density fluctuation driven by coherent modes such as kink/tearing mode<sup>10</sup> (going through the LO laser chord) (i.e., in the far-forward mode). This will be demonstrated in detail in Sec. III. In the forward mode of this scattering diagnostic, the angle between the MB CO<sub>2</sub> laser and each LO CO<sub>2</sub> laser determines both the corresponding scattering angle  $\theta_s$  and the wavenumber  $k$  (according to the Bragg condition,  $k = 2k_i \sin(\theta_s/2)$ ). The scattering angles are very small ( $\theta_s \leq 0.3^\circ$ ), so each HgCdTe detector (D1 and D2) must be picking up the forward scattered signals (mixed with both the LO CO<sub>2</sub> laser and far-forward scattering signals produced by the LO CO<sub>2</sub> laser) focused onto it. So, both forward and far-forward scattering signals can be detected simultaneously. It is noted that each LO CO<sub>2</sub> laser (mixed with scattered signals) acts independently, and there is not some kind of array effect being used. The maximum  $k_{\perp}$  of far-forward scattering signals is determined by the width of the LO beam  $w_{LO}$ , i.e.,  $k_{\perp} \leq \pi/w_{LO}$  ( $k_{\perp} \leq 3 \text{ cm}^{-1}$  in this paper and no wavenumber resolution). It is noted here that the density fluctuation measured by the far-forward scattering is line-averaged, and far-forward scattering signals are sensitive to any coherent mode going through the LO CO<sub>2</sub> laser chord.

## III. IDENTIFICATION OF THE QCM BEING MEASURED BY LO CO<sub>2</sub> LASER FAR-FORWARD SCATTERING

In the EAST experiment, both broadband  $k_{\perp} = 10 - 30 \text{ cm}^{-1}$  density fluctuation and coherent mode can be measured

simultaneously by the EAST tangential CO<sub>2</sub> laser collective scattering system. It is no doubt that  $k_{\perp} = 10\text{--}30\text{ cm}^{-1}$  density fluctuation is from the MB CO<sub>2</sub> laser forward scattering signals. Wavenumber separation is obvious between the long wavelength coherent mode (such as kink/tearing mode) and broadband (intermediate and high)- $k$  density fluctuation. So, the coherent mode is not expected to be measured directly by the collective scattering system in the forward mode. Thus, we would consider the far-forward scattering scheme,<sup>24,25</sup> which is just due to LO CO<sub>2</sub> laser scattering. We only blocked the MB CO<sub>2</sub> laser through using Dump 1 (see Fig. 1) in an EDA/small ELM H mode plasma discharge (#55749). It is noted here that the Dump is not the detector, and it is only used to absorb all the CO<sub>2</sub> laser energy focusing onto it. A low frequency mode (see Fig. 2) has been observed in the cross-power and the squared coherence spectrum of two scattering signals measured by LO1 and LO2 CO<sub>2</sub> laser collective scattering systems, respectively. This experimental result proves that the coherent mode (such as the QCM in this paper) is measured by each LO CO<sub>2</sub> laser far-forward scattering diagnostic. The power spectrum analysis of these far-forward scattering signals for #55749 (not shown) implies that the power of  $k_{\perp} \leq 3\text{ cm}^{-1}$  broadband density fluctuation is extremely small (much smaller than the usual MB CO<sub>2</sub> laser forward scattering signals) except at the QCM frequency. This is consistent with the theoretical result that the coherent mode is from a small wavenumber feature which could have large amplitude. It is worth pointing out that both forward (measuring

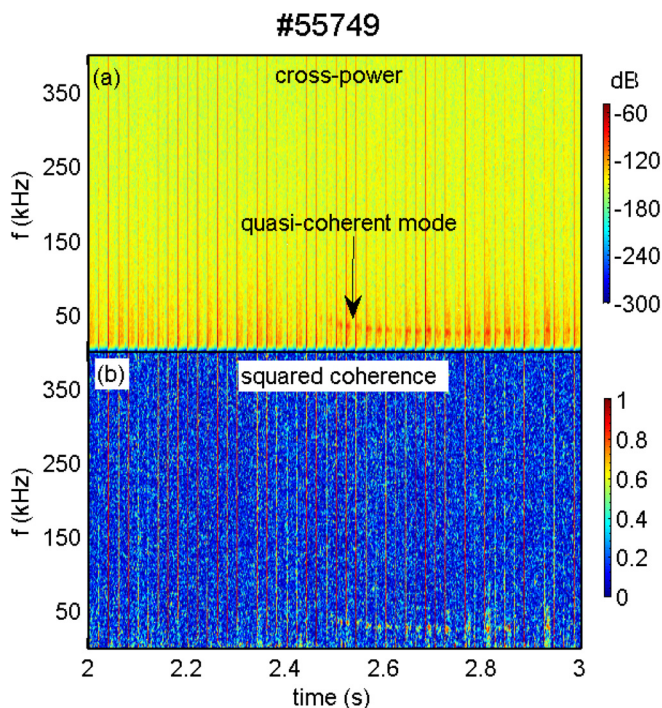


**FIG. 2.** A low frequency mode has been observed in the analysis of (a) cross-power and (b) squared-coherence between LO1 and LO2 CO<sub>2</sub> laser scattering signals, which is carried out with a frequency resolution of 1 kHz, 8 ensembles, and a noise level of  $N = 1/8 = 0.125$ .

$k_{\perp} = 10\text{--}30\text{ cm}^{-1}$  density fluctuation) and far-forward (only being sensitive to the coherent mode) scattering signals can be measured simultaneously by the scattering system when we only use Dump 2 instead of using Dump 1 to block the MB CO<sub>2</sub> laser.

## IV. EXPERIMENTAL RESULTS AND DISCUSSION

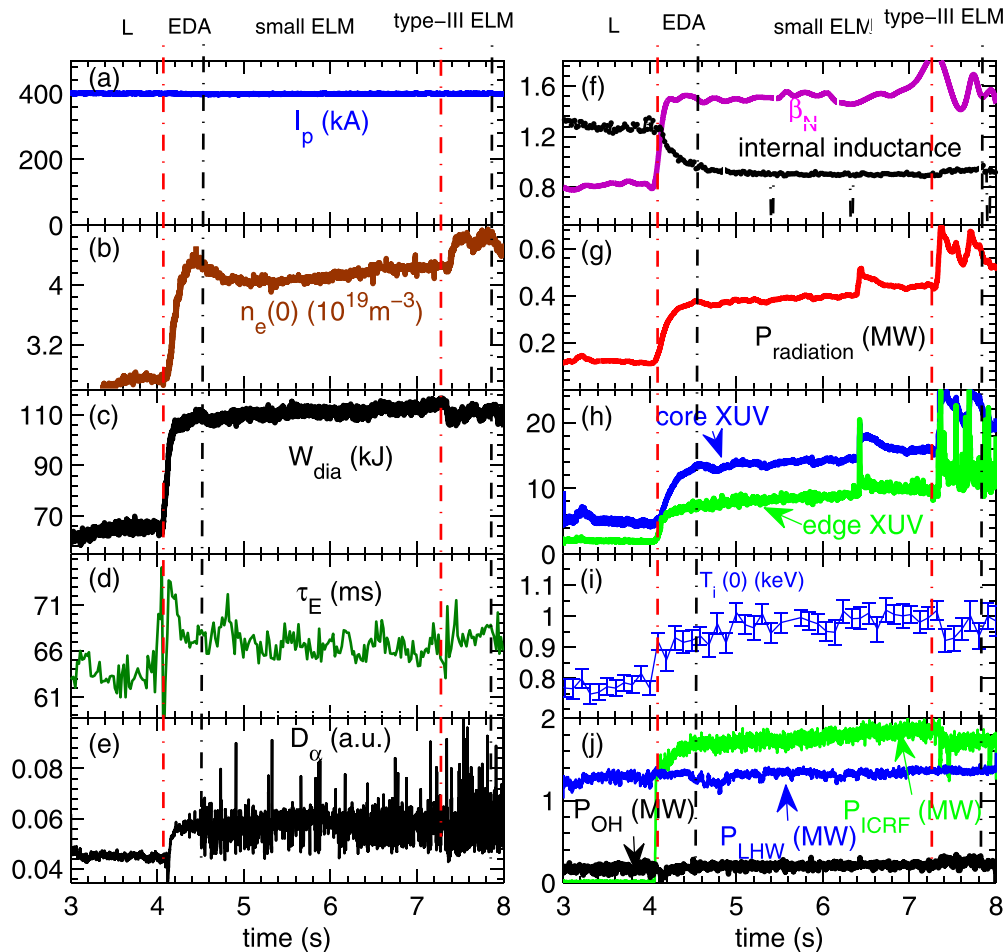
### A. Overview of EDA/small ELM H mode plasma discharge

Figure 3 shows a common EDA/small ELM H mode plasma discharge (#39465) in EAST. The set of H mode deuterium plasmas in which the observation was made has a minor radius of  $a \approx 0.45\text{ m}$ , a major radius of  $R_0 \approx 1.85\text{ m}$ , a lower single null configuration, a toroidal magnetic field of 1.8 T, and a plasma current of 400 kA [see Fig. 3(a)]. Auxiliary heating from a lower hybrid wave (LHW) with a source power around 1.1 MW is available at  $t = 3\text{--}8\text{ s}$  [see Fig. 3(j)]. LHW can deposit and mainly heat plasma electrons in a broad plasma region  $r/a \approx 0.15\text{--}0.8$ .<sup>26</sup> The 27 MHz ion cyclotron resonance frequency (ICRF) wave with the source power about 2 MW was applied to heat plasma ions with H minority on-axis heating in deuterium majority plasmas from  $t = 4\text{ s}$  [see Fig. 3(j)]. Plasma L-H transition occurs at  $t \approx 4.1\text{ s}$ , when the following signals show an obvious increase in the H mode phase: central line-averaged electron density  $n_e(0)$  [see Fig. 3(b)], plasma stored energy  $W_{dia}$  [see Fig. 3(c)], energy confinement time  $\tau_E$  [see Fig. 3(d)], normalized beta  $\beta_N$  [see Fig. 3(f)], plasma total radiation power [see Fig. 3(g)], core and edge extreme ultraviolet (XUV) [see Fig. 3(h)], and core region ion temperature [see Fig. 3(i)]. Meanwhile, the internal inductance [see Fig. 3(f)] has a decrease. The lower level of internal inductance in the H mode phase implies that the plasma current density is not peaked off-center in core plasmas (i.e., no weak or reverse magnetic shear). Therefore, the internal transport barrier probably does not occur.<sup>1</sup> From the  $D_x$  signal shown in Fig. 3(e), we can know that the initial plasma is the enhanced  $D_x$  (EDA) H mode,<sup>17</sup> and then, small ELMs occur and last from 4.69 s to 7.3 s. At last, the plasma evolves to the high frequency type-III ELM. This is related to the increase in total radiation power [see Fig. 3(g)], which was measured by the EAST resistive bolometer.<sup>27</sup>

### B. The observation of the QCM by the CO<sub>2</sub> laser collective scattering system

In the EAST experiment, the QCM [see Figs. 4(a) and 4(b)] has been observed in the spectrogram of CO<sub>2</sub> laser scattered signals during the EDA/small ELM H mode phase (LHW coupled with ICRF auxiliary heating). The spectrum of the QCM is quite narrow at all times with both frequencies  $f \approx 26.5\text{ kHz}$  and  $\Delta f/f \approx 0.15$ . Note that  $\Delta f$  is the full frequency width at half maximum power of density fluctuation. This QCM appears at  $t \approx 4.117\text{ s}$  (about 17 ms after the plasma low-high confinement (LH) transition time) and disappears in the high frequency type-III ELM H mode plasma phase at about  $t = 7.318\text{ s}$  [see Figs. 4(a) and 4(b)]. The frequency of this QCM, extracted from channel 2 density fluctuation, is shown in Fig. 4(c). It is noted that this frequency is the same as that extracted from channel 1 density fluctuation. Figure 4(d) plots the power at QCM frequency. The frequency of

#39465



**FIG. 3.** An overview of an EDA H mode plasma discharge (#39465): (a) plasma current  $I_p$  (kA), (b) central line-averaged electron density  $n_e(0)$ , (c) plasma stored energy  $W_{dia}$ , (d) energy confinement time  $\tau_E$ , (e)  $D_\alpha$  signal, (f) normalized beta  $\beta_N$  and internal inductance  $\ell_i$ , (g) total radiation power  $P_{radiation}$ , (h) core and edge XUV, (i) central ion temperature  $T_i(0)$ , and (j) source power of LHW, ICRF, and Ohm.

the QCM sweeps down quickly from  $f \approx 56$  kHz at  $t = 4.117$  s to  $f \approx 26.5$  kHz at  $t = 4.69$  s and sustains 26.5 kHz during the small ELM phase. Meanwhile, the plasma toroidal rotation velocity increases from  $\Delta V_t(t = 4.117\text{s}) \approx 3$  to  $\Delta V_t(t = 4.69\text{s}) \approx 24$  km/s [see Fig. 4(e)], where  $\Delta V_t$  was measured by the EAST imaging x-ray crystal spectrometer diagnostic.<sup>28,29</sup> Note that  $\Delta V_t(t)$  satisfies  $\Delta V_t(t) = V_t(t) - V_t(t = 1.5\text{s})$ . The analysis from Mirnov coil arrays<sup>30</sup> shows that the toroidal mode number of the QCM is  $n = -1$  (see Fig. 5). Note that  $n < 0$  represents that this mode rotates along the electron diamagnetic drift direction in the lab frame. Due to the Nyquist limit of toroidal mode number detection (i.e.,  $|n| \leq 8$ ), the actual mode number should be  $n \approx 1 + 8 \times N$ , where  $N$  is an integer. We know that mode frequency  $f_{lab}$  in the lab frame consists of real frequency  $f_{real}$  and Doppler shift  $f_{Doppler}$  ( $f_{Doppler} = \frac{k_r V_t}{2\pi}$ ), i.e.,  $f_{lab} = f_{real} + f_{Doppler}$ , and the latter is usually dominant.<sup>12</sup> Therefore, the decreasing amount of QCM

frequency has been considered to be mainly from the change in its Doppler shift, i.e.,  $\delta f_{Doppler} = \frac{n}{2\pi R_0} \times (\Delta V_t(t = 4.117\text{s}) - \Delta V_t(t = 4.69\text{s})) \approx f(t = 4.117\text{s}) - f(t = 4.69\text{s})$ . This result shows that the toroidal mode number of the QCM is  $n \approx 17$ . This also matches the relation  $n \approx 1 + 8 \times N$ . It is noted here that the poloidal mode number of the QCM is not available.

The QCM also has been observed in the ELM-free H mode plasmas with only LHW heating. Figure 6 shows an overview of such discharge (#38333), for which we have done supplementary analysis. This shot in which the observation of the QCM is made has a plasma current of 400 kA [see Fig. 6(a)] and a toroidal magnetic field of 1.8 T. The time range of interest is  $t = 6.165 - 6.65$  s when the plasma current is in the flat-top phase at first and then ramps down at a rate about 190 kA/s. Meanwhile, the line-averaged electron density increases all the time until the high-low confinement (HL) transition time at  $t = 6.75$  s [see Fig.

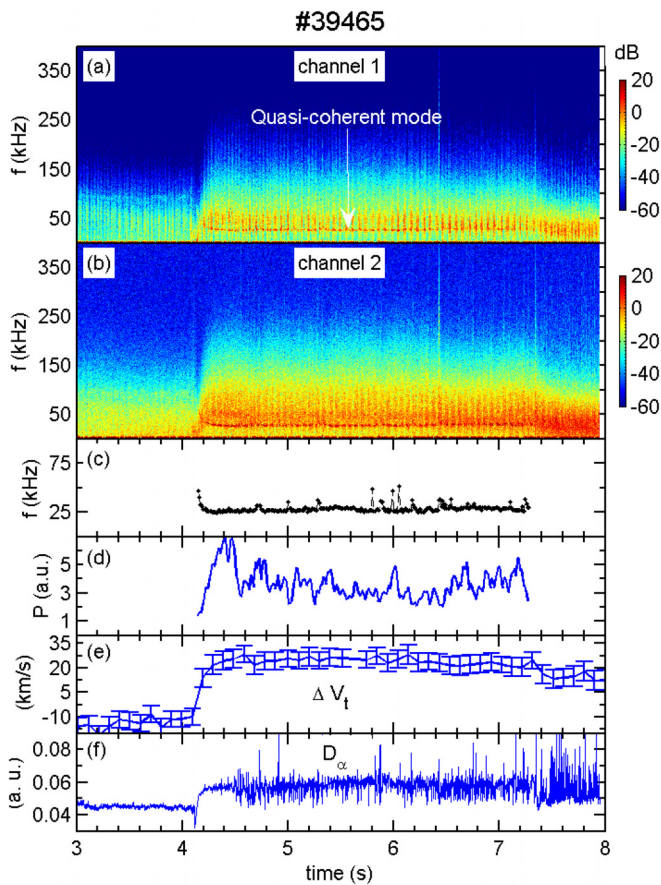


**FIG. 4.** Frequency spectrum of density fluctuation signals from (a) channel 1 and (b) channel 2. Time evolution of (c) QCM frequency extracted from channel 2 density fluctuation, (d) scattering power at the QCM frequency, (e) plasma toroidal rotation velocity, and (f)  $D_\alpha$  signal.

6(b)]. The stored energy, on the other hand, has an initial increase from 54 kJ to 83 kJ and then decreases (following the drop of plasma current) to 61 kJ before HL transition [see Fig. 6(c)]. The time evolution of the poloidal beta  $\beta_p$  is similar to that of electron density.  $\beta_p$  increases continuously from  $\beta_p \sim 0.5$  to  $\beta_p \sim 0.9$  just before the HL transition [see Fig. 6(d)]. The drop of the internal inductance  $\ell_i$  values [see Fig. 6(d)] probably implies that no ITB exists in the ELM-free H mode plasma phase.  $D_\alpha$  signals shown in Fig. 6(e) imply that plasma LH transition time is  $t \approx 6.165$  s. The source power of LHW is around 1.1 MW during the existing time of the QCM [see Fig. 6(f)]. The QCM is simultaneously observed in all channels of  $\text{CO}_2$  laser scattering signals [see Fig. 6(g), for example]. This mode occurs at the time  $t \approx 6.165$  s (50 ms after the LH transition), exists during the ELM-free H mode phase ( $t \approx 6.165 - 6.65$  s), and disappears when the plasma comes into the type-III ELM H mode phase. This is similar to those observations in #39465. The frequency of the QCM [see Fig. 6(h)], extracted from channel 2 density fluctuation, sweeps down from  $f \approx 60$  kHz to  $f \approx 26$  kHz. Note that the extracted frequency of the QCM from channel 1 (not shown) is

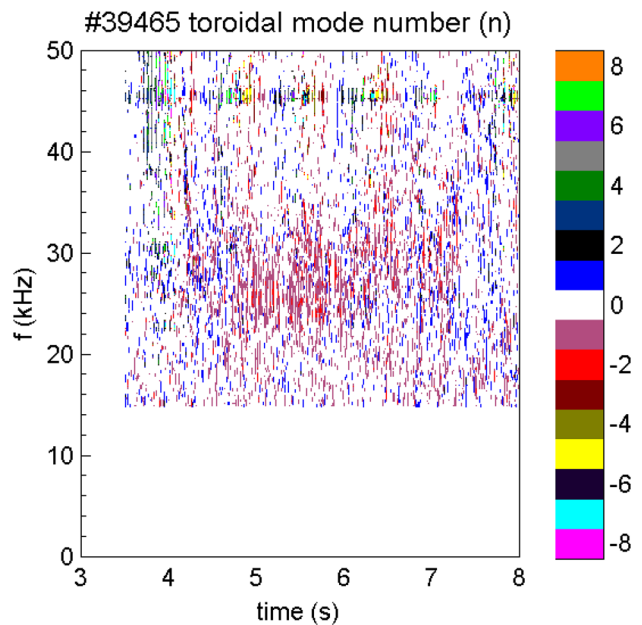


**FIG. 5.** The calculation of the QCM's toroidal mode number through using the Fourier transform to get the phase difference among Mirnov coil arrays.

the same as that from channel 2. The power of the QCM, extracted from both channel 1 and channel 2 density fluctuation signals, is plotted in Fig. 6(i), separately. QCM power from both channel 1 and channel 2 shows an initial increase in general during the plasma current flat-top phase and then decreases continuously following the ramp-down plasma current. Plasma absorbed power can be calculated through  $P_{\text{absorb}} = P_{\text{LHW}} + P_{\text{OH}} - P_{\text{radiation}}$ . Although the source power of LHW and Ohm is stable, the absorbed power shows a slow decrease due to the continuous increase in radiation power. This may be related to the transition from the ELM-free to the type-III ELM phase. Here, it is clear that the QCM can appear in either the EDA/small ELM or ELM-free phase in the auxiliary heating of LHW alone or LHW coupling with ICRF and disappear in the type-III ELM H mode phase.

### C. Comparison of the QCM in EAST with the QC mode in C-Mod tokamak

In C-Mod tokamak, a continuous QC mode was found in the EDA H mode phase for either Ohmic or ICRF heating plasmas. The spectrum is quite narrow at all times with  $\Delta f/f \approx 0.2$ . The QC mode has been identified to be responsible for the enhanced particle transport in edge plasmas. The QC mode localizes in the steep density gradient (pedestal) region of the plasma edge. The Mirnov coil signals mounted on the reciprocating probe<sup>20,21</sup> measure the poloidal fluctuating field component,  $\tilde{B}_\theta$ , of this QC mode. Snipes *et al.* extrapolate their  $\tilde{B}_\theta$  to last closed flux surface (LCFS) ( $B_\theta \approx 5$  G) after fitting the fluctuation measurements to a decaying exponential, as expected in the scrape-off-layer. So, this QC mode is considered to be an

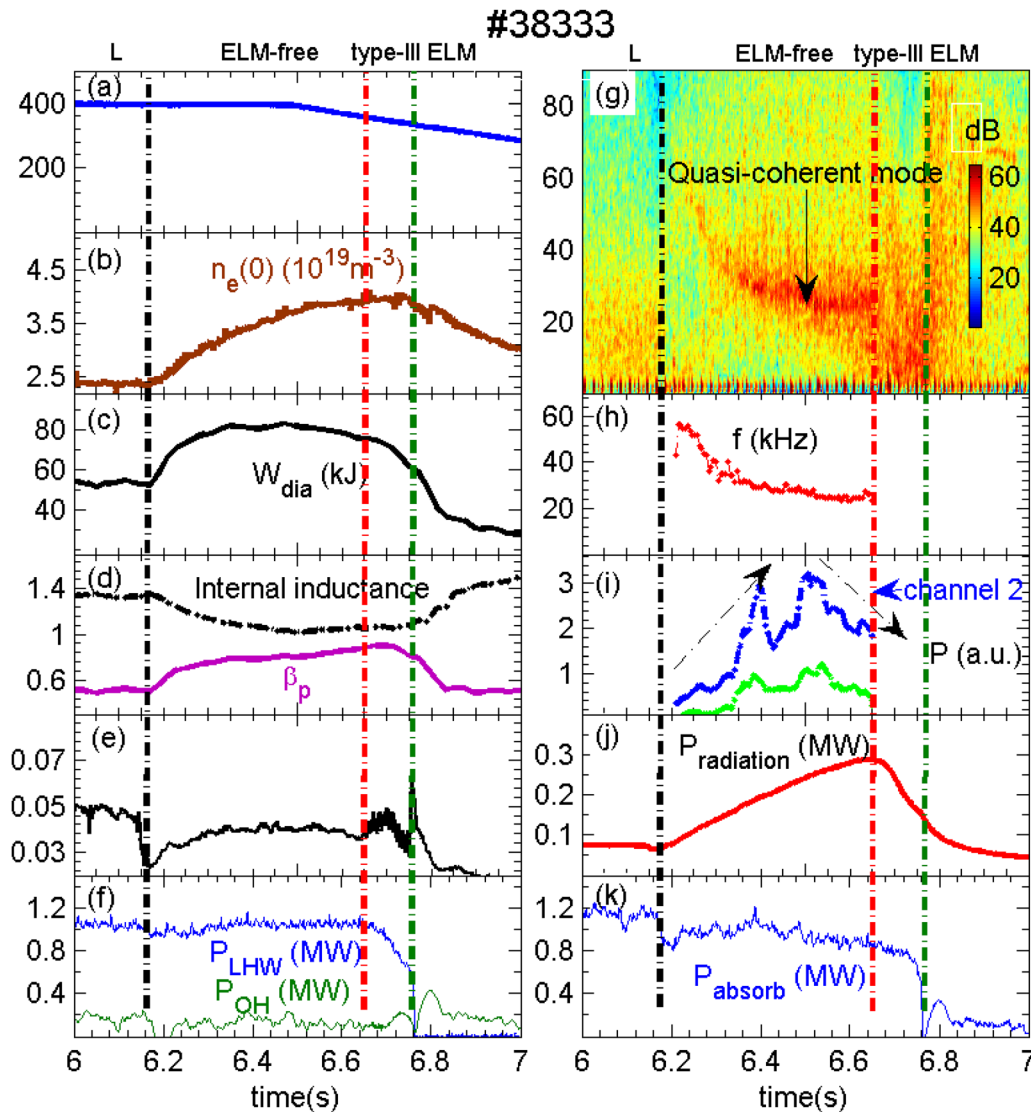


**FIG. 6.** Time evolution of (#38333) (a) plasma current  $I_p$  (kA), (b) central line-averaged density  $n_e(0)$ , (c) stored energy  $W_{dia}$ , (d) internal inductance  $\ell_i$  and poloidal beta  $\beta_p$ , (e)  $D_z$  signal, (f) the source power of LHW and Ohm, (g) frequency spectrum of channel 2 density fluctuation signals, (h) QCM frequency extracted from (g), (i) QCM power extracted from channel 1 and channel 2 scattering signals, separately, (j) total radiation power  $P_{radiation}$ , and (k) plasma absorbed power  $P_{absorb}$ .

electromagnetic mode. The toroidal mode number of the QCM is proposed as  $n \approx k_\theta R B_\theta / B_\phi \approx 30$ ,<sup>20</sup> and this corresponds to a toroidal wavenumber  $k_t = n/R = 30/68 = 0.44 \text{ cm}^{-1}$ . This mode exhibits a high frequency ( $f \approx 100 \text{ kHz}$ ) and sinusoidal characteristics in both density and magnetic fluctuations, with typical wave numbers  $k_R \approx 3 - 6 \text{ cm}^{-1}$  and  $k_\theta \approx 1.3 \text{ cm}^{-1}$  (mid-plane).<sup>17</sup>

The measurement of the QCM in the EAST tokamak has been made with the LO CO<sub>2</sub> laser far-forward scattering signals (see Sec. III). It is mentioned here again that the far-forward scattering diagnostic makes a line-averaged measurement of the QCM and cannot localize QCM radially. However, the

toroidal mode number of the QCM ( $n \approx 17$ ) is much higher than that of the kink/tearing mode ( $n \sim 1-4$ ). So, it is unlikely that the Mirnov coils (situated more than 80 mm outside the LCFS) would be able to resolve anything other than the QCM with a magnetic fluctuating component at the edge due to the rapid attenuation of the fluctuating magnetic signal (moving out in radius) at a higher wavenumber. Therefore, the Mirnov coil data provide some indirect evidence in support of edge localization of the QCM. The electron density profile, measured by the EAST W-band microwave reflectometer,<sup>31</sup> is shown in Fig. 7. The LH transition time is  $t_{LH} \approx 4.1 \text{ s}$ . It can be found that the electron density gradient is much bigger at  $t > t_{LH}$  (EDA H mode phase, e.g.,  $t = 4.12, 4.14, \text{ and } 4.17 \text{ s}$ ) than at  $t < t_{LH}$  (L mode phase, e.g.,  $t = 4$

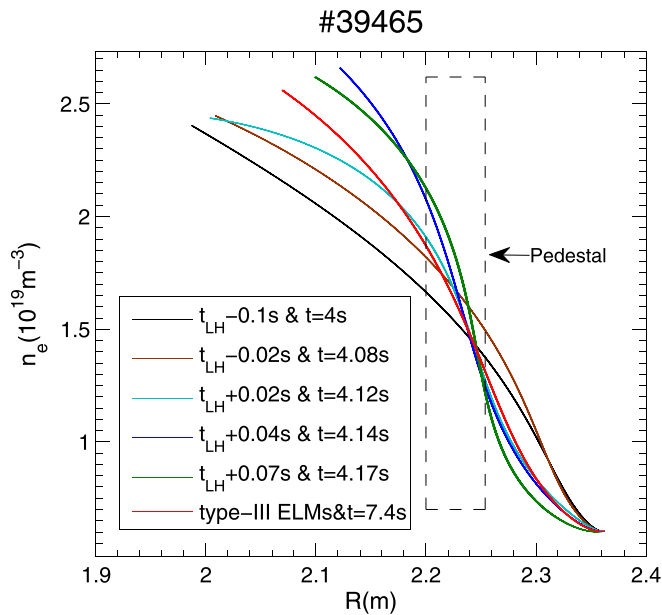


**FIG. 7.** The evolution of electron density profile at around LH transition time  $t_{LH} = 4.1$  s.

and 4.08 s) for  $R = 2.2\text{--}2.25$  m (steep edge density profile region). The appearance of the QCM (17 ms after plasma LH transition) is just accompanied by the build-up of steep edge pedestal. The QCM mode disappears in the type-III ELM phase, when the plasma electron density gradient is lower than that of the EDA/small ELM phase and is higher than that of the L mode phase (see Fig. 7). It is important to note that QCM power increases significantly [see Fig. 4(d)] when the electron density profile becomes steeper and steeper in the pedestal region as the time evolution for  $t = 4.12\text{--}4.17$  s. Moreover, Fig. 6(i) shows a continuous increase in QCM power in the plasma current flat-top and ELM-free phase, when the plasma profile usually should become more and more steeper. These results imply that the occurrence QCM is related to the steep electron density profile. This also indirectly supports that the QCM localizes in the edge pedestal region. The EAST QCM can be observed in either the EDA/small ELM or ELM-free phase in the auxiliary heating of LHW alone or LHW coupling with ICRF. Since the QCM has a high toroidal mode number  $n \approx 17$  and the Mirnov coils are situated more than 80 mm outside the LCFS, the attenuation of magnetic fluctuation driven by the QCM should be very fast. However, the QCM can be observed in the spectrum of Mirnov signals. So, the QCM should be an electromagnetic mode. The increase in QCM power [see Fig. 6(i)] is consistent with the increase in the  $D_x$  signal in the plasma current flat-top phase. This is more obvious in the initial EDA H mode phase for shot #39465 [see Fig. 4(d)]. Comparison with that in the EDA H mode phase (#39465), QCM power, shows an obvious decrease in the small ELM H mode phase [see Fig. 4(d)]. Moreover, the power of the QCM in the ELM-free H mode phase [see Fig. 6(e)] is lower than that in the EDA/small ELM H mode phase [see Fig. 4(d)]. This is consistent with a

smaller value of  $D_x$  in the ELM-free phase [see Fig. 6(e)] than that in the EDA/small ELM phase [see Fig. 4(d)]. Therefore, the QCM power decreases in turn in the EDA H mode phase, small ELM phase, and ELM-free phase. The QCM cannot be found in the type-III ELM phase. Moreover, the appearance of the QCM is at a high line-averaged electron density condition, i.e.,  $\bar{n}_e(0) > 0.6 \times n_G$ , where  $n_G$  is the Greenwald density limit. So, this QCM may transport particle outwardly. The LO beam CO<sub>2</sub> laser far-forward scattering diagnostic, being used to measure the QCM, can measure  $k_{\perp} < 3 \text{ cm}^{-1}$  density fluctuation (see Sec. III), and the toroidal wave number of the QCM is  $k_t \approx n/R = 17/185 = 0.092 \text{ cm}^{-1}$ . The QCM frequency in the C-Mod tokamak is  $f \approx 100 \text{ kHz}$ , which is nearly 3.8 times of QCM frequency ( $f \approx 26.5 \text{ kHz}$ ) in EAST. As mentioned previously that QCM frequency  $f_{lab}$  consists of real frequency  $f_{real}$  and Doppler shift  $f_{Doppler}$ , i.e.,  $f_{lab} = f_{real} + f_{Doppler}$ . The QCM's Doppler shift can be calculated according to  $f_{Doppler} = k_t V_t / 2\pi$ . The toroidal rotation velocity  $V_t$  has been given in the C-Mod EDA H mode phase,<sup>32</sup> and its value is  $V_t \sim 10 \text{ km/s}$ . In this paper, only  $\Delta V_t(t) = V_t(t) - V_t(t = 1.5 \text{ s})$  has been given by the EAST imaging x-ray crystal spectrometer diagnostic.  $\Delta V_t(t)$  is around 24 km/s in the EDA/small ELM phase. Due to the lack of  $V_t(t = 1.5 \text{ s})$ , we still do not know the exact value of  $V_t$  in the EDA/small ELM H mode phase. Since no obvious momentum (such as neutral beam injection) injects into the plasmas, the generation of toroidal rotation should be nearly spontaneous in both C-Mod [Ohmic or ICRF (less momentum injection)] and EAST plasmas (LHW or LHW+ICRF). Therefore, their toroidal rotation velocity  $V_t$  may be close to each other. Previous analysis shows that the toroidal wavenumber for the C-Mod QC mode ( $k_t = 0.44 \text{ cm}^{-1}$ ) is nearly 4.8 times for the EAST QCM ( $k_t \approx 0.092 \text{ cm}^{-1}$ ). Different  $k_t$  between the EAST QCM and C-Mod QC mode may result in different  $f_{Doppler}$ . This may be the major factor leading to different  $f_{lab}$  between EAST QCM and C-Mod QC modes. However, their  $f_{real}$  may be close to each other. The EAST QCM bandwidth ( $\Delta f/f \approx 0.15$ ) is very close to that ( $\Delta f/f \approx 0.2$ ) of the C-Mod QC mode. Since the frequency of the EAST QCM ( $f \approx 26.5 \text{ kHz}$ ) is much higher than that of the typical kink/tearing mode ( $f < 10 \text{ kHz}$ ) in EAST,<sup>30,33</sup> this mode cannot be an internal kink mode or a tearing mode. Both the appearance and power of the EAST QCM are greatly related to a build-up of edge steep pedestal. This suggests that the EAST QCM may also be a ballooning mode like QC mode in C-Mod.

Based on the above results, several similar features have been found between the EAST QCM and C-Mod QC mode, which include the following: (a) both the EAST QCM and C-Mod QC mode accompany a LH confinement regime transition; (b) the frequency of both modes sweeps down at first and then localizes at a stable value; (c) both quasi-coherent modes can be observed in EDA H mode plasmas; (d) the possible wavenumber of the EAST QCM ( $k_{\perp} < 3 \text{ cm}^{-1}$ ) does not conflict with the  $k_R$  and  $k_{\theta}$  components of the C-Mod QC mode; (e) both the EAST QCM and C-Mod QC mode have magnetic fluctuation components and should be an electromagnetic mode; (f) the EAST QCM may transport particles outwardly like the C-Mod QC mode; (g) the occurrence of both the EAST QCM and C-Mod QC mode is related to the steep edge density profile and the EAST



QCM may also be a ballooning mode like the QC mode in C-Mod; (h) the  $f_{real}$  of the EAST QCM and C-Mod QC mode may be close to each other; (i) the bandwidth of the EAST QCM is close to that of the C-Mod QC mode; and (j) both the EAST QCM and C-Mod QC mode are observed at high electron density. In summary, many similar basic features (e.g., real frequency, frequency bandwidth, location in the plasmas, being related to the density gradient driven, effects on transport, dominant wavenumber, and the occurrence time) have been found between the EAST QCM and C-Mod QC mode. These features support that the EAST QCM may be fundamentally the same type mode as the C-Mod QC mode.

The QCM real frequency can be calculated through using  $f_{real} = k_{\theta} V_{*e} / 2\pi = k_{\theta} \partial_r P_e / (2\pi e B n_e)$ . So, the impact factors on  $f_{real}$  are  $k_{\theta}$ ,  $P_e$ ,  $B$ ,  $n_e$ , and so on. Toroidal magnetic field  $B_t$  and the  $R$  in the EDA H mode phase are  $B_t = 5.3$  T and  $R = 0.68$  m in C-Mod and  $B_t = 2$  T and  $R = 1.85$  m in EAST for centre plasmas. Because we do not know the value of  $k_{\theta}$  and  $P_e$ , we cannot calculate the value of EAST QCM real frequency and make a real frequency comparison between the EAST QCM and C-Mod QC mode. We will study this in the future.  $q_{95}$  (the safety factor at the normalized poloidal flux  $\Psi = 0.95$ ) is a parameter that matters for EDA existence in the C-Mod tokamak, which is around  $q_{95} = 3.5$ . In the EAST tokamak,  $q_{95}$  is around 4.5 when the QCM exists in the plasma for #39465 and increases continuously from 4.4 to 5 when the QCM exists in the plasma for #38333. Due to the lack of profiles  $T_{e,i}$ , safety factor  $q$ , etc., a detailed study of the contribution of the QCM on the electron energy/particle transport will be carried out quantitatively in a future paper.

## V. SUMMARY

In summary, we have studied the QCM in detail for the first time through using the EAST tangential CO<sub>2</sub> laser collective scattering diagnostic. The QCM is identified to be measured by the scattering diagnostic in the far-forward mode. The QCM has been observed at high electron density during both EDA/small ELM and ELM-free H mode phases. The QCM has been observed to have a typical frequency  $f \approx 26.5$  kHz, have toroidal mode number  $n \approx 17$ , driven density fluctuation ( $k_{\perp} < 3$  cm<sup>-1</sup>), and magnetic fluctuation and rotates along with the electron diamagnetic drift velocity direction in the lab frame. Further analysis of Mirnov and reflectometer signals supports that the QCM locates in the edge pedestal region, and QCM power is related to the pedestal density gradient. QCM power has also been found to be related to the  $D_x$  signal, which may imply that the QCM can outwardly transport particles radially. Detailed comparisons of the EAST QCM and C-Mod QC mode support that the EAST QCM is likely to be the same type mode as the C-Mod QC mode. The effect of the QCM on the electron energy/particle transport will be carried out quantitatively in the future.

## ACKNOWLEDGMENTS

The author thanks Professor Q. Q. Yu, C. X. Yu, D. L. Brower, W. X. Ding, W. Chen, X. Q. Xu, and Z. X. Wang for their useful discussions. This work was supported by the National

Natural Science Foundation of China under Contract Nos. 11475222, 11505228, 11875286, 11735016, and 11575238 and the National Key Development Project under Contract No. 2016YFA0400600.

## REFERENCES

- <sup>1</sup>E. J. Doyle, W. A. Houlberg, Y. Kamada, V. Mukhovatov, T. H. Osborne, A. Polevoi, G. Bateman, J. W. Connor, J. G. Cordey, T. Fujita et al., *Nucl. Fusion* **47**, S18–S127 (2007).
- <sup>2</sup>X. Wan, J. G. Li, Y. Liu, X. L. Wang, V. Chan, C. G. Chen, X. R. Duan, P. Fu, X. Gao, K. M. Feng, S. L. Liu, Y. T. Song, P. D. Weng, B. N. Wan, F. R. Wan, H. Y. Wang, S. T. Wu, M. Y. Ye, Q. W. Yang, G. Y. Zheng, G. Zhuang, Q. Li, and CFETR Team, *Nucl. Fusion* **57**, 102009 (2017).
- <sup>3</sup>J. E. Menard, L. Bromberg, T. Brown, T. Burgess, D. Dix, L. El-Guebaly, T. Gerrity, R. J. Goldston, R. J. Hawryluk, R. Kastner, C. Kessel, S. Malang, J. Minervini, G. H. Neilson, C. L. Neumeyer, S. Prager, M. Sawan, J. Sheffield, A. Sternlieb, L. Waganer, D. Whyte, and M. Zarnstorff, *Nucl. Fusion* **51**, 103014 (2011).
- <sup>4</sup>Y. Ren, W. Guttenfelder, S. M. Kaye, E. Mazzucato, R. E. Bell, A. Diallo, C. W. Domier, B. P. LeBlanc, K. C. Lee, D. R. Smith, and H. Yuh, *Phys. Plasmas* **19**, 056125 (2012).
- <sup>5</sup>E. Mazzucato, D. R. Smith, R. E. Bell, S. M. Kaye, J. C. Hosea, B. P. LeBlanc, J. R. Wilson, P. M. Ryan, C. W. Domier, N. C. Luhmann, Jr., H. Yuh, W. Lee, and H. Park, *Phys. Rev. Lett.* **101**, 075001 (2008).
- <sup>6</sup>Y. Ren, W. Guttenfelder, S. M. Kaye, E. Mazzucato, R. E. Bell, A. Diallo, C. W. Domier, B. P. LeBlanc, K. C. Lee, M. Podesta, D. R. Smith, and H. Yuh, *Nucl. Fusion* **53**, 083007 (2013).
- <sup>7</sup>Y. Ren, W. X. Wang, B. P. LeBlanc, W. Guttenfelder, S. M. Kaye, S. Ethier, E. Mazzucato, K. C. Lee, C. W. Domier, R. Bell, D. R. Smith, and H. Yuh, *Phys. Plasmas* **22**, 110701 (2015).
- <sup>8</sup>Y. Ren, S. M. Kaye, E. Mazzucato, W. Guttenfelder, R. E. Bell, C. W. Domier, B. P. LeBlanc, K. C. Lee, N. C. Luhmann, Jr., D. R. Smith, and H. Yuh, *Phys. Rev. Lett.* **106**, 165005 (2011).
- <sup>9</sup>Y. Ren, E. Belova, N. Gorelenkov, W. Guttenfelder, S. M. Kaye, E. Mazzucato, J. L. Peterson, D. R. Smith, D. Stutman, K. Tritz, W. X. Wang, H. Yuh, R. E. Bell, C. W. Domier, and B. P. LeBlanc, *Nucl. Fusion* **57**, 072002 (2017).
- <sup>10</sup>P. J. Sun, Y. D. Li, Y. Ren, X. D. Zhang, G. J. Wu, L. Q. Xu, R. Chen, Q. Li, H. L. Zhao, J. Z. Zhang, T. H. Shi, Y. M. Wang, B. Lyu, L. Q. Hu, J. Li, and EAST Team, *Nucl. Fusion* **58**, 016003 (2018).
- <sup>11</sup>M. Jiang, W. L. Zhong, Y. Xu, Z. B. Shi, W. Chen, X. Q. Ji, X. T. Ding, Z. C. Yang, P. W. Shi, A. S. Liang, J. Wen, J. Q. Li, Y. Zhou, Y. G. Li, D. L. Yu, Y. Liu, Q. W. Yang, and HL-2A Team, *Nucl. Fusion* **58**, 026002 (2018).
- <sup>12</sup>P. J. Sun, Y. D. Li, Y. Ren, X. D. Zhang, G. J. Wu, B. Lyu, T. H. Shi, L. Q. Xu, F. D. Wang, Q. Li, J. Z. Zhang, L. Q. Hu, J. G. Li, and EAST Team, *Plasma Phys. Controlled Fusion* **60**, 025019 (2018).
- <sup>13</sup>L. Bardóczi, T. L. Rhodes, T. A. Carter, A. Bañón Navarro, W. A. Peebles, F. Jenko, and G. McKee, *Phys. Rev. Lett.* **116**, 215001 (2016).
- <sup>14</sup>H. Y. W. Tsui, K. Rypdal, C. P. Ritz, and A. J. Wootton, *Phys. Rev. Lett.* **70**, 2565 (1993).
- <sup>15</sup>R. E. Slusher, C. M. Surko, J. F. Valley, T. Crowley, E. Mazzucato, and K. McGuire, *Phys. Rev. Lett.* **53**, 667 (1984).
- <sup>16</sup>T. Estrada, A. Alonso, A. A. Chmyga, N. Dreval, L. Eliseev, C. Hidalgo, A. D. Komarov, A. S. Kozachok, L. Krupnik, and A. V. Melnikov, *Plasma Phys. Controlled Fusion* **47**, L57–L63 (2005).
- <sup>17</sup>A. Mazurenko, M. Porkolab, D. Mossessian, J. A. Snipes, X. Q. Xu, and W. M. Nevins, *Phys. Rev. Lett.* **89**, 225004 (2002).
- <sup>18</sup>J. L. Terry, N. P. Basse, I. Cziegler, M. Greenwald, O. Grulke, B. LaBombard, S. J. Zweben, E. M. Edlund, J. W. Hughes, L. Lin, Y. Lin, M. Porkolab, M. Sampsell, B. Veto, and S. J. Wukitch, *Nucl. Fusion* **45**, 1321–1327 (2005).
- <sup>19</sup>D. A. Mossessian, R. J. Groebner, R. A. Moyer, T. H. Osborne, J. W. Hughes, M. Greenwald, A. Hubbard, and T. L. Rhodes, *Phys. Plasmas* **10**, 689–698 (2003).
- <sup>20</sup>J. A. Snipes, B. LaBombard, M. Greenwald, I. H. Hutchinson, J. Irby, Y. Lin, A. Mazurenko, and M. Porkolab, *Plasma Phys. Controlled Fusion* **43**, L23–L30 (2001).

- <sup>21</sup>B. LaBombard, T. Golfinopoulos, J. L. Terry, D. Brunner, E. Davis, M. Greenwald, J. W. Hughes, and Alcator C-Mod Team, *Phys. Plasmas* **21**, 056108 (2014).
- <sup>22</sup>B. Chen, X. Q. Xu, T. Y. Xia, M. Porkolab, E. Edlund, B. LaBombard, J. Terry, J. W. Hughes, S. F. Mao, M. Y. Ye, and Y. X. Wan, *Nucl. Fusion* **57**, 116025 (2017).
- <sup>23</sup>R. E. Slusher and C. M. Surko, *Phys. Fluids* **23**, 472 (1980).
- <sup>24</sup>C. B. Deng and D. L. Brower, *Rev. Sci. Instrum.* **81**, 10D503 (2010).
- <sup>25</sup>W. X. Ding, L. Lin, J. R. Duff, D. L. Brower, and J. S. Sarf, *Rev. Sci. Instrum.* **83**, 10 (2012).
- <sup>26</sup>M. H. Li, B. J. Ding, E. H. Kong, L. Zhang, X. J. Zhang, J. P. Qian, N. Yan, X. F. Han, J. F. Shan, and F. K. Liu, *Chin. Phys. B* **20**, 125202 (2011).
- <sup>27</sup>Y. M. Duan, L. Q. Hu, S. T. Mao, K. Y. Chen, S. Y. Lin, and EAST Diagnostics Team, *Rev. Sci. Instrum.* **83**, 093501 (2012).
- <sup>28</sup>Y. J. Shi, F. D. Wang, B. N. Wan, M. Bitter, S. Lee, J. Bak, K. Hill, J. Fu, Y. Y. Li, and W. Zhang, *Plasma Phys. Controlled Fusion* **52**, 085014 (2010).
- <sup>29</sup>B. Lu, F. Wang, Y. Shi, M. Bitter, K. W. Hill, S. G. Lee, J. Fu, Y. Li, and B. Wan, *Rev. Sci. Instrum.* **83**, 10E130 (2012).
- <sup>30</sup>T. H. Shi, B. N. Wan, B. Shen, Y. W. Sun, J. P. Qian, L. Q. Hu, X. Z. Gong, G. J. Liu, Z. P. Luo, G. Q. Zhong, L. Q. Xu, J. Z. Zhang, S. Y. Lin, Y. X. Jie, F. D. Wang, B. Lv, and EAST Team, *Plasma Phys. Controlled Fusion* **55**, 055007 (2013).
- <sup>31</sup>Y. M. Wang, X. Gao, B. L. Ling, S. B. Zhang, T. Zhang, X. Han, S. C. Liu, Z. X. Liu, Y. Liu, A. Ti, and EAST Team, *Fusion Eng. Des.* **88**, 2950 (2013).
- <sup>32</sup>J. E. Rice, W. D. Lee, E. S. Marmor, N. P. Basse, P. T. Bonoli, M. J. Greenwald, A. E. Hubbard, J. W. Hughes, I. H. Hutchinson, A. Ince-Cushman, J. H. Irby, Y. Lin, D. Mossessian, J. A. Snipes, S. M. Wolfe, S. J. Wukitch, and K. Zhurovich, *Phys. Plasmas* **11**, 2427 (2004).
- <sup>33</sup>L. Q. Xu, L. Q. Hu, K. Y. Chen, E. Z. Li, F. D. Wang, G. Q. Zhong, Y. J. Chen, Y. Xi, and EAST Team, *Plasma Phys. Controlled Fusion* **55**, 032001 (2013).